

# Observation of the scaling dimension of fractional quantum Hall anyons

A. Veillon,<sup>1</sup> C. Piquard,<sup>1</sup> P. Glidic,<sup>1</sup> Y. Sato,<sup>1</sup> A. Aassime,<sup>1</sup>  
A. Cavanna,<sup>1</sup> Y. Jin,<sup>1</sup> U. Gennser,<sup>1</sup> A. Anthore,<sup>1,2</sup> and F. Pierre<sup>1</sup>

<sup>1</sup> *Université Paris-Saclay, CNRS, Centre de Nanosciences et de Nanotechnologies, 91120, Palaiseau, France*

<sup>2</sup> *Université Paris Cité, CNRS, Centre de Nanosciences et de Nanotechnologies, F-91120, Palaiseau, France*

Unconventional quasiparticles emerging in the fractional quantum Hall regime [1] present the challenge of observing their exotic properties unambiguously. Although the fractional charge of quasiparticles has been demonstrated since nearly three decades [2–4], the first convincing evidence of their anyonic quantum statistics has only recently been obtained [5, 6] and, so far, the so-called scaling dimension that determines the quasiparticles’ propagation dynamics remains elusive. In particular, while the non-linearity of the tunneling quasiparticle current should reveal their scaling dimension, the measurements fail to match theory, arguably because this observable is not robust to non-universal complications [7–11]. Here we achieve an unambiguous measurement of the scaling dimension from the thermal to shot noise cross-over, and observe a long-awaited agreement with expectations. Measurements are fitted to the predicted finite temperature expression involving both the quasiparticles scaling dimension and their charge [11, 12], in contrast to previous charge investigations focusing on the high bias shot noise regime [13]. A systematic analysis, repeated on multiple constrictions and experimental conditions, consistently matches the theoretical scaling dimensions for the fractional quasiparticles emerging at filling factors  $\nu = 1/3$ ,  $2/5$  and  $2/3$ . This establishes a central property of fractional quantum Hall anyons, and demonstrates a powerful and complementary window into exotic quasiparticles.

Exotic quasiparticles could provide a path to protected manipulations of quantum information [14]. Yet their basic features are often challenging to ascertain experimentally. The broad variety of quasiparticles emerging in the regimes of the fractional quantum Hall effect constitutes a prominent illustration [1]. These are characterized by three unconventional properties [15, 16]: *(i)* their charge  $e^*$  is a fraction of the elementary electron charge  $e$ , *(ii)* their anyonic quantum statistics is different from that of bosons and fermions, and *(iii)* the dynamical response to their injection or removal along the propagative edge channels is peculiar, ruled by a ‘scaling dimension’  $\Delta$  different from the trivial  $\Delta = 1/2$  of non-interacting electrons. In the simplest Laughlin quantum Hall states, at filling factors  $\nu = 1/(2n+1)$  ( $n \in \mathbb{N}$ ), the fractional anyon quasiparticles have a charge  $e^* = \nu e$ , an exchange phase  $\theta = \nu\pi$  and a scaling dimension  $\Delta = \nu/2$ . Despite four decades of uninterrupted investigations of the quantum Hall physics, experimental confirmations of the predicted scaling dimension remain lacking, including for Laughlin fractions.

Such a gap may appear surprising since  $\Delta$  plays a role in most transport phenomena across quantum point contacts (QPC), the basic building block of quantum Hall circuits. Indeed, the elementary tunneling process itself consists in the removal of a quasiparticle on one side of a QPC and its reinjection on the other side, whose time correlations are set by  $\Delta$  [15, 16]. In Luttinger liquids, the quasiparticles’ scaling dimension is related to the interaction strength, also referred to as the interaction parameter  $K$ , which notably determines the non-linear  $I - V$  characteristics across a local impurity [17]. Consequently, the knowledge of  $\Delta$  is often a prerequisite to connect a transport observable with a property of interest. Furthermore, as straightforwardly illustrated in the Hong-Ou-

Mandel setup [18–20],  $\Delta$  naturally rules time controlled manipulations of anyons, which are required in the perspective of topologically protected quantum computation based on braiding [14]. In this work, the scaling dimension of fractional quantum Hall quasiparticles is disclosed from the thermal noise to shot noise crossover, as recently proposed [11, 12]. The observed good agreement with universal predictions experimentally establishes the theoretical understanding and completes our picture of the exotic fractional quantum Hall anyons.

## Characterizing exotic quasiparticles.

The first unconventional property of quantum Hall quasiparticles that has been established is their fractional charge  $e^*$ . Consistent values were observed by multiple experimental approaches, with the main body of investigations based on shot noise measurements across a QPC [2–4, 21–27]. In this case, the scaling dimension can be canceled out, leaving only  $e^*$ , by focusing on the ratio between shot noise and tunneling current (the Fano factor) at high bias voltages. The non-standard braiding statistics of fractional quasiparticles turned out more challenging to observe. Convincing evidences were obtained only recently, through Aharonov-Bohm interferometry [5, 28] as well as from noise measurements in a ‘collider’ geometry [6, 29–31]. Note that whereas the latter strategy is particularly versatile, the noise signal is also entangled with the scaling dimension [19, 20, 32, 33], which complicates a quantitative determination of the anyon exchange phase  $\theta$  [29]. Finally, the quasiparticles scaling dimension was previously investigated through measurements of the non-linear current-voltage characteristics of a QPC [34–36]. However, no reliable value of  $\Delta$  could be obtained for the fractional quasiparticles of the quantum Hall regime (see [37] for an observation in a circuit quantum simula-

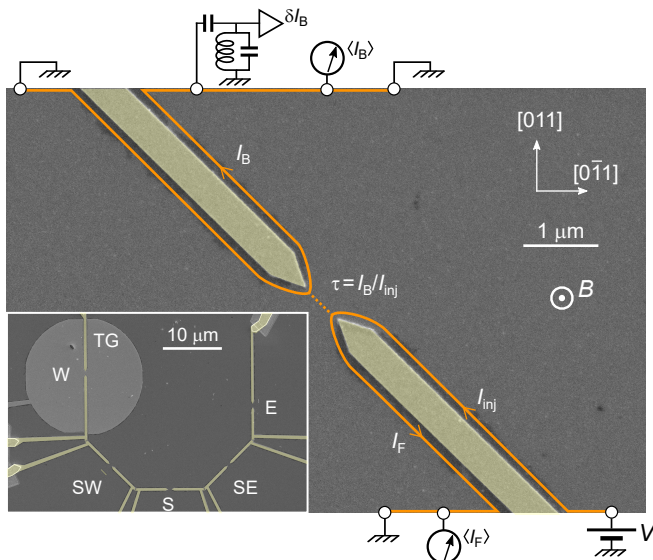


FIG. 1. **Experimental setup.** Electron-beam micrographs of the measured Ga(Al)As device. QPCs are formed in the 2DEG by applying a negative voltage to the metallic gates colored yellow. The sample includes five QPCs (E, SE, S, SW and W) along different crystallographic orientations (inset, see Supplementary Fig. S1 for larger-scale images). Among those, QPC<sub>W</sub> differs by the presence of closely surrounding metallic gate (TG) extending over a  $10\ \mu\text{m}$  radius (see Supplementary Fig. S2 for close-up images). Quasiparticle tunneling takes place between chiral quantum Hall edge channels shown as orange lines with arrows (main panel, QPC<sub>SW</sub>). The auto-correlations in back-scattered (tunneling) current  $\langle \delta I_B^2 \rangle$  are measured for all QPCs. QPC<sub>E</sub> also includes a noise amplification chain for the forward current fluctuations  $\delta I_F$  (not shown), hence allowing for the additional measurements of  $\langle \delta I_F^2 \rangle$  and  $\langle \delta I_B \delta I_F \rangle$ .

tor, and [38] for a good match on the  $I(V)$  of tunneling electrons across a ( $\nu = 1$ ) – ( $\nu = 1/3$ ) interface). Indeed, the  $I - V$  characteristics is generally found at odds with the standard model of a chiral Luttinger liquid with a local impurity (see e.g. [13, 16, 39, 40] and references therein). Most often a fit is impossible, or only by introducing extra offsets and with unrealistic values for  $e^*$  and  $\Delta$  [30, 35, 36, 41].

The puzzling  $I - V$  situation motivated multiple theoretical investigations. A simple possible explanation for the data-theory mismatch is that the shape of the QPC potential, and therefore the quasiparticle tunneling amplitude, is impacted by external parameters, such as an electrostatic deformation induced by a change in the applied bias voltage, the temperature or the tunneling current itself [9]. Other possible non-universal complications include an energy-dependent tunneling amplitude [10], additional edge modes either localized [7] or propagative [42, 43], and Coulomb interactions between different edges [8]. In this context, the scaling dimension was connected to different, arguably more robust proposed observables such as delta- $T$  noise [44, 45], thermal

to shot noise crossover [11, 12] and thermal Fano factor [46].

A proven strategy to cancel out non-universal behaviors consists in considering a well-chosen ratio of transport properties, as illustrated by the Fano factor  $F$  successfully used to extract  $e^*$ . Recently, it was proposed that the same  $F$  could also give access to the quasiparticles' scaling dimension, when focusing on the lower bias voltage regime where the crossover between thermal noise and shot noise takes place [11, 12]. As further detailed later-on, the predicted evolution of  $F$  along the crossover exhibits a markedly different width and overall shape depending on the value of  $\Delta$ .

The present investigation implements the characterization of the scaling dimension from the Fano factor crossover on four different quantum Hall quasiparticles [15, 47]: (i) the  $e^* = e/3$  quasiparticles at  $\nu = 1/3$  and along the outer edge channel at  $\nu = 2/5$ , of predicted  $\Delta = 1/6$ ; (ii) the  $e^* = e/5$  quasiparticles along the inner edge channel at  $\nu = 2/5$ , of predicted  $\Delta = 3/10$ ; (iii) the  $e^* = e/3$  quasiparticles at  $\nu = 2/3$ , of predicted  $\Delta = 1/3$ ; (iv) the electrons at  $\nu = 3$  of trivial  $\Delta = 1/2$ .

### Experimental implementation.

The measured sample is shown in Fig. 1 together with a schematic representation of the setup. It is nanofabricated by e-beam lithography from a Ga(Al)As two-dimensional electron gas (2DEG). The experiments are performed at  $T \approx 30\ \text{mK}$ , if not specified otherwise, and the sample is immersed in a strong perpendicular magnetic field corresponding to the quantum Hall effect at filling factors  $\nu \in \{1/3, 2/5, 2/3, 3\}$ . In these quantum Hall regimes, the current propagates chirally along the sample edges, as schematically pictured by lines with arrows. The buried 2DEG is electrically connected through large ohmic contacts (depicted as circles) positioned  $100 - 200\ \mu\text{m}$  away from the QPCs. Quantum point contacts are formed in the 2DEG by field effect, within the opening of metallic split gates (yellow) deposited at the surface, on top of an intercalated layer of  $\text{HfO}_2$ . We characterize a QPC by the gate-controlled transmission ratio  $\tau \equiv I_B / I_{\text{inj}}$ , with  $I_B$  the back-scattered current and  $I_{\text{inj}}$  the incident current along the partially transmitted edge channel (the other channels at  $\nu = 2/5$  and  $\nu = 3$  are either fully reflected or transmitted). The sample includes five QPCs of different orientations with respect to the Ga(Al)As crystal. A specific QPC is individually addressed by completely closing all the other ones. The split gates geometry is nominally identical for all QPCs. QPC<sub>W</sub>, of identical orientation as QPC<sub>E</sub>, also includes an additional top-gate, which allows us to locally tune the 2DEG density, and increases the screening of long-range Coulomb interactions [8, 48] and the sharpness of the edge confinement potential [42].

The central noise signal  $S$  is measured using two home-made cryogenic amplifiers (one schematically shown). These are connected through nearly identical  $L - C$  tank circuits. A reliable and independent knowledge of the

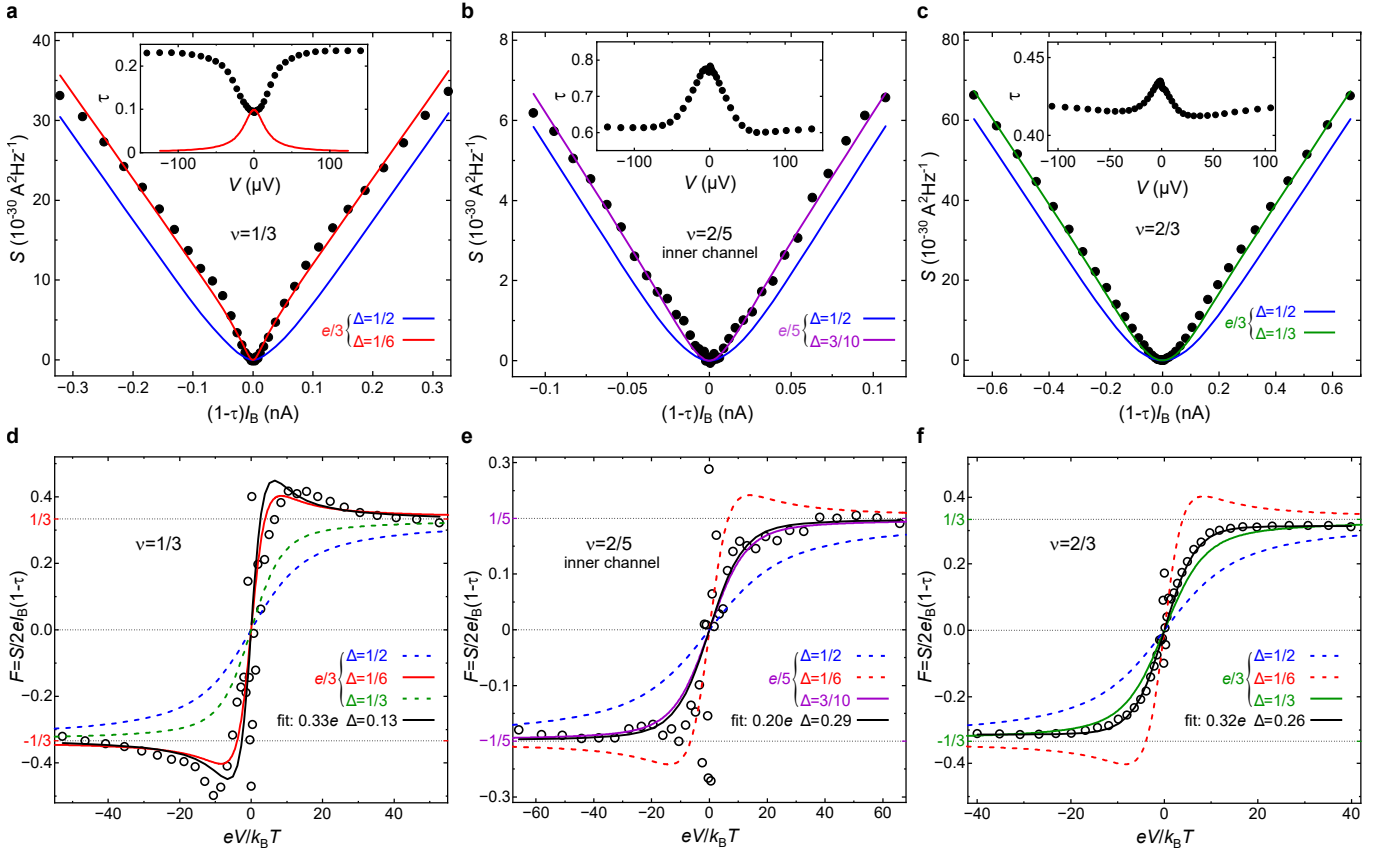


FIG. 2. **Thermal to shot noise crossover.** Data-theory comparison at  $\nu = 1/3$  (a,d), on the inner  $e^2/15h$  channel of  $\nu = 2/5$  (b,e) and at  $\nu = 2/3$  (c,f). **a,b,c**, Excess noise  $S$  versus normalized tunnel current  $(1-\tau)I_B$ . Symbols are measurements. Blue lines are phenomenological predictions of Eq. 1 ( $\Delta = 1/2$ , predicted  $e^*$ ). Red, purple and green lines are predictions of Eq. 2 (predicted  $\Delta$  and  $e^*$ ). Inset:  $\tau(V)$  measurements are shown as symbols. The  $\nu = 1/3$  prediction (red line) differs strongly from these. **d,e,f**, Fano factor  $F \equiv S/2eI_B(1-\tau)$  vs  $eV/k_B T$ . Measurements (symbols) agree best with the predictions of Eq. 2 computed using the predicted quasiparticle scaling dimension  $\Delta$  (colored continuous lines) than using the electron scaling dimension  $1/2$  (blue dashed lines), both assuming the predicted  $e^*$ . Black continuous lines are fits using  $e^*$  and  $\Delta$  as free parameters.

electronic temperature within the device and of the gain of the amplification chain are particularly crucial for the analysis of the thermal to shot noise crossover. This was achieved through the robust fluctuation-dissipation relation to thermal noise (Methods). One cryogenic amplifier (top-left in Fig. 1) measures the back-scattered (tunneling) current noise  $\langle \delta I_B^2 \rangle$  for any addressed QPCs. The second cryogenic amplifier (not shown) measures the forward current fluctuations  $\delta I_F$  transmitted specifically across QPC<sub>E</sub>. Therefore, for QPC<sub>E</sub> we also have access to the noise in the forward current  $\langle \delta I_F^2 \rangle$  and to the cross-correlations between forward and back-scattered current fluctuations  $\langle \delta I_B \delta I_F \rangle$ . Besides increasing the signal to noise ratio, this allows one to ascertain that  $\langle \delta I_B^2 \rangle$  matches the more robust cross-correlation signal [49]. In practice, the additional noise introduced by the amplification chains is removed by focusing on the excess noise with respect to zero bias:  $S(V) \equiv \langle \delta I^2 \rangle(V) - \langle \delta I^2 \rangle(0)$ .

### Scaling dimension characterization.

In previous characterizations of the charge  $e^*$  of fractional quantum Hall quasiparticles, the shot noise is usually plotted as a function of the back-scattered current  $I_B$ , and  $e^*$  is extracted by matching the high-bias slope  $\partial S / \partial I_B$  with  $2e^*(1-\tau)$ , where  $1-\tau$  corrects for tunneling correlations at finite  $\tau$  [50]. Even in this representation, which adequately puts the emphasis on the larger high-bias shot noise, a visually discernible and experimentally relevant difference allows one to discriminate between predicted and trivial  $\Delta$ , as illustrated in the first row of Fig. 2. Blue continuous lines display the excess shot noise of quasiparticles of trivial  $\Delta = 1/2$  and of charge  $e/3$  (a,c) or  $e/5$  (b), which is given by the broadly used phenomenological expression [13, 50]:

$$S_{1/2} = 2e^* I_B (1-\tau) \left[ \coth \frac{e^* V}{2k_B T} - \frac{2k_B T}{e^* V} \right]. \quad (1)$$

The continuous lines of a different color in the main panels of Fig. 2a,b,c show the excess noise for the predicted quasiparticle scaling dimension  $\Delta = 1/6$  (red, (a)),

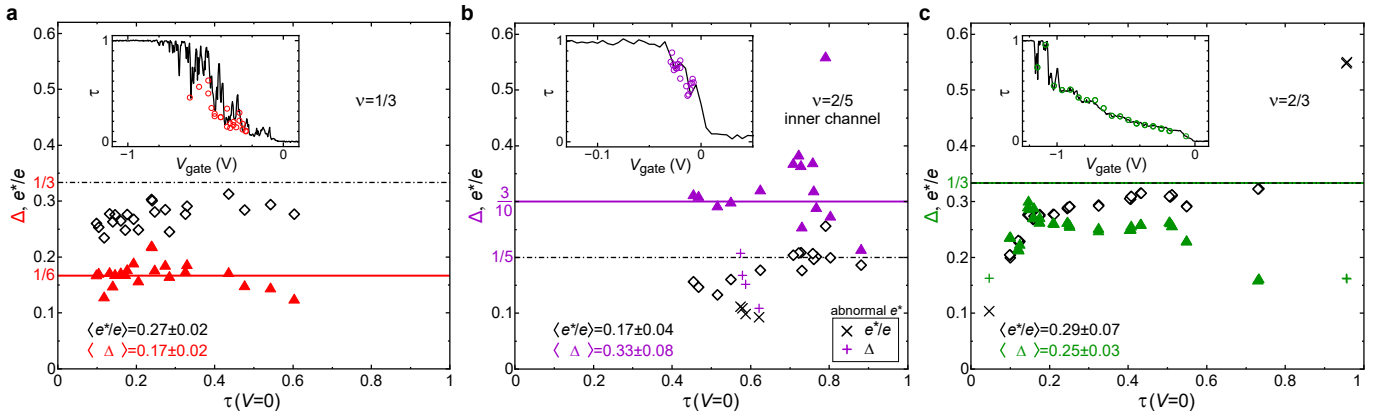


FIG. 3. **Scaling dimension vs QPC tuning.** Scaling dimension ( $\blacktriangle$ ) and charge ( $\diamond$ ) obtained along illustrative spans in gate voltage ( $V_{\text{gate}}$ ) of QPC<sub>E</sub> are plotted vs  $\tau(V=0)$  (**a**,  $\nu = 1/3$ ; **b**, inner channel at  $\nu = 2/5$ ; **c**,  $\nu = 2/3$ ). At  $\nu = 2/5$  (**b**) and  $\nu = 2/3$  (**c**), a few points are shown as different symbols (+, x). They are associated with anomalously low  $e^* \lesssim e_{\text{th}}^*/2$  or high  $e^* \gtrsim 3/2e_{\text{th}}^*$  charge compared to the predicted charge  $e_{\text{th}}^*$ . Horizontal lines represent the theoretical predictions for  $\Delta$  (continuous) and  $e^*/e$  (dash-dot). Inset: Separately measured  $\tau(V_{\text{gate}})$  sweeps (continuous lines), and individual noise measurement tunings (symbols). For  $\nu = 1/3$ , a noticeable difference is due to a slightly different magnetic field setting ( $\delta B \simeq -0.5$  T) between  $V_{\text{gate}}$  sweep and noise measurements.

$\Delta = 3/10$  (purple, (b)) and  $\Delta = 1/3$  (green, (c)) obtained from [7, 11, 12]:

$$S_{\Delta} = 2e^* I_B (1 - \tau) \text{Im} \left[ \frac{2}{\pi} \psi \left( 2\Delta + i \frac{e^* V}{2\pi k_B T} \right) \right], \quad (2)$$

with  $\psi$  the digamma function and  $1 - \tau$  the ad hoc amplitude factor used for extracting  $e^*$  from the shot noise slope at high bias. (Note that Eq. 2 reduces to Eq. 1 at  $\Delta = 1/2$ .) The difference is strongest for the quasiparticles  $\{e/3, \Delta = 1/6\}$  predicted at  $\nu = 1/3$ , with an apparent width of the thermal-shot noise crossover more than twice narrower than for  $\Delta = 1/2$  (Fig. 2a). The difference is smaller for the quasiparticles  $\{e/5, \Delta = 3/10\}$  and  $\{e/3, \Delta = 1/3\}$  since  $\Delta$  is closer to  $1/2$  (Fig. 2b,c). Nevertheless, as can be straightforwardly inferred from the scatter of the data, it remains in all cases larger than our experimental resolution on the noise. One can already notice that the illustrative shot noise measurements shown in Fig. 2a,b,c are closer to the parameter-free prediction of Eq. 2 with the expected  $\Delta$ . Note that this agreement is accompanied by a puzzling  $I - V$  characteristics as previously mentioned (see  $\tau(V)$  in insets and also in Supplementary Fig. S6).

For the present aim of characterizing  $\Delta$  from the thermal-shot noise crossover, the Fano factor  $F \equiv S/2eI_B(1 - \tau)$  of bounded amplitude at high bias is better suited [11, 12]. It is plotted versus the relevant variable  $eV/k_B T$  (see Eq. 2) in the lower row of Fig. 2, with symbols and colored lines corresponding to the noise displayed in the panel immediately above. Importantly, the effect of  $\Delta < 1/2$  on  $F$  is not limited to an increased slope at low bias, which could in principle be attributed to a temperature lower than the separately characterized  $T$ , but results in marked changes in the overall shape of  $F(eV/k_B T)$ . In particular, for  $\Delta = 1/6$  the Fano factor

is non-monotonous (red line in Fig. 2d). The increasing steepness while reducing  $\Delta$  combined with an overall change of shape facilitates the extraction of this parameter from a fit of the noise data using Eq. 2. Qualitatively, the value of  $F$  at large bias solely reflects  $e^*/e$ , the overall cross-over shape (such as a non-monotonous dependence at  $\Delta < 1/4$ ) solely involves  $\Delta$ , and the low-bias slope is a combination of both  $e^*$  and  $\Delta$ . The results of such fits (minimizing the data-Eq. 2 variance) are shown as black continuous lines in Fig. 2d,e,f, together with the corresponding fitting parameters  $e^*$  and  $\Delta$  (the temperature being fixed to the separately determined  $T = 31$  mK). In order to firmly establish the extracted values of the quasiparticles scaling dimension, and to test the universal character of our observations, the same procedure was systematically repeated on numerous device settings, as detailed in the next section.

### Robustness of observations.

Focusing on the Fano factor cancels out some of the non-universal behaviors, but not all of them. Of particular concern are the disorder-induced resonances, which could result in a Coulomb-dominated sequential tunneling with a strong effect on the Fano factor. This is likely to happen in the fractional quantum Hall regime where QPCs often exhibit narrow peaks and dips in their transmission. Accordingly, for some gate voltages we find that an accurate fit of the noise data is not possible with Eq. 2, whatever  $e^*$  and  $\Delta$ . In such cases, the resulting fitted values are meaningless. This was transparently addressed with a maximum variance criteria between data and best fit. If the fit-data variance is higher than this, the extracted  $e^*$  and  $\Delta$  are discarded (see Methods). This same procedure was systematically applied to all the noise measurements per-

formed over a broad span of gate voltages controlling  $\tau$  (the full data set, including discarded fits and analysis code, is available in a Zenodo deposit).

The values of  $e^*$  and  $\Delta$  obtained while spanning the gate voltage of the same QPC<sub>E</sub> are shown versus  $\tau(V=0)$  in Fig. 3, for each of the three probed fractional quasiparticles (see Supplementary Information for electrons at  $\nu=3$ ). We find remarkably robust scaling dimensions (and charges), close to the predictions shown as horizontal lines. In particular, although the nature of the tunneling quasiparticles is eventually going to change at  $\tau \rightarrow 1$ , we observe that  $\Delta$  and  $e^*$  extracted with Eq. 2 (which is exact only at  $\tau \ll 1$ ) remain relatively stable over a broad range of  $\tau$ . Such a stability matches previous  $e^*$  measurements, including a particularly steady  $e/5$  [51]. Figure 3a shows data points obtained in the  $\nu=1/3$  plateau. A statistical analysis of the ensemble of these points yields  $\langle \Delta \rangle \simeq 0.167$  with a spread of  $\sigma_\Delta \simeq 0.023$ , which is to be compared with the prediction  $\Delta = 1/6 \simeq 0.1667$ . The data-prediction agreement on  $\Delta$  is at the level, if not better, than that on  $e^*$  (often found slightly lower than expected). Similar sweeps are shown in Fig. 3b,c for the inner channel of conductance  $e^2/15h$  at  $\nu=2/5$  (b), and at  $\nu=2/3$  (c). Note that a few data points at  $\nu=2/5$  and at  $\nu=2/3$  are displayed as pairs of ‘x’ ( $e^*/e$ ) and ‘+’ ( $\Delta$ ) instead of open and full symbols (Fig. 3, panels b and c). This indicates an anomalous fitted value of the charge  $e^*$ , off by about 50% or more from the well-established prediction  $e_{\text{th}}^* = e/5$  and  $e_{\text{th}}^* = e/3$  respectively (dash-dot line). Because this suggests a non-canonical QPC behavior with substantial consequences on the mean and spread of  $\Delta$ , we chose not to include these relatively rare points in the data ensemble analysis of  $\Delta$  (they remain included in the statistical analysis of  $e^*$ ). For this reduced data set composed of fifteen measurements along the inner channel at  $\nu=2/5$ , we obtain  $\langle \Delta \rangle \simeq 0.327$  with a spread of  $\sigma_\Delta \simeq 0.078$ , which is to be compared with the predicted  $\Delta = 3/10$  of  $e/5$  quasiparticles. Lastly, at  $\nu=2/3$ , the gate voltage sweep shown in Fig. 3c gives  $\langle \Delta \rangle \simeq 0.249$  and  $\sigma_\Delta \simeq 0.029$ , close to the predicted  $\Delta = 1/3 \simeq 0.33$ .

The robustness and generic character of these  $\Delta$  observations are further established by repeating the same procedure in different configurations: (i) on several QPCs, with different orientations with respect to the Ga(Al)As crystal; (ii) for multiple temperatures  $T$ ; (iii) for several top gate voltages  $V_{\text{tg}}$  controlling the density in the vicinity of QPC<sub>W</sub>; (iv) by changing the magnetic field, both along the  $\nu=1/3$  plateau and to  $\nu=2/5$  on the

outer edge channel. Figure 4 recapitulates all our measurements (283 in total), including conventional electrons at  $\nu=3$ . Each point represents the average value  $\langle e^*/e \rangle$  ( $\diamond$ ) or  $\langle \Delta \rangle$  ( $\blacktriangle$ ) and the corresponding standard deviation obtained while broadly spanning the gate voltage of the indicated QPC (individually extracted  $e^*$  and  $\Delta$  are provided in Supplementary Information). See also Methods for consistent conclusions from an alternative fitting procedure where  $\Delta$  is the only free parameter ( $e^*$  being

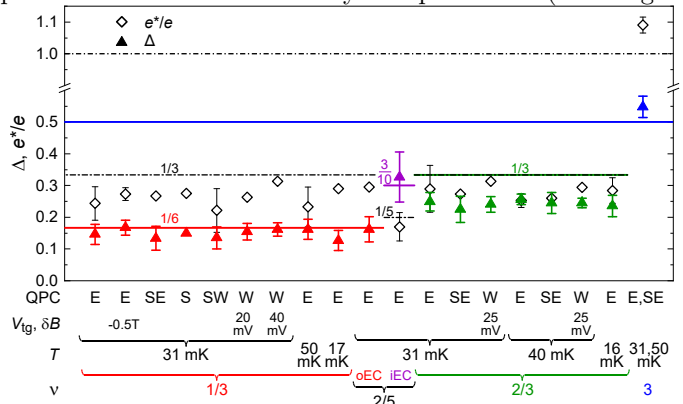


FIG. 4. **Summary of observations.** Each symbol with error bars represents the mean and standard deviation of the ensemble of  $\Delta$  ( $\blacktriangle$ ) and  $e^*/e$  ( $\diamond$ ) extracted along one gate voltage span of a QPC, such as those shown in Fig. 3. The horizontal axis indicates the experimental conditions: label of the QPC (E, SE, S, SW, W), voltage  $V_{\text{tg}}$  applied to the top gate (TG) around QPC<sub>W</sub>, magnetic field shift  $\delta B$  from the center of the plateau (if any), temperature  $T$ , filling factor  $\nu$  and for  $\nu=2/5$  the probed edge channel (inner ‘iEC’ or outer ‘oEC’) with different colors for different predicted quasiparticles.

fixed to the well-established prediction, and focusing on low voltages  $e^*|V| \leq 2k_{\text{B}}T$ ).

### Conclusion.

Fano factor measurements previously used to investigate the charge of tunneling quasiparticles also allow for a consistent determination of their scaling dimension, from the width and specific shape of  $F(eV/k_{\text{B}}T)$ . Combined with a systematic approach, the resulting observations of  $\Delta$  establish long-lasting theoretical predictions for the fractional quantum Hall quasiparticles at  $\nu=1/3$ ,  $2/5$  and  $2/3$ . This approach could be generalized to other quasiparticles, and in particular to shed light on the non-abelian quantum Hall quasiparticles predicted at even-denominator filling factors [52].

- [1] Stern, A. Anyons and the quantum Hall effect—A pedagogical review. *Ann. Phys.* **323**, 204–249 (2008).  
 [2] Goldman, V. J. & Su, B. Resonant Tunneling in the Quantum Hall Regime: Measurement of Fractional Charge. *Science* **267**, 1010–1012 (1995).

- [3] de Picciotto, R. *et al.* Direct observation of a fractional charge. *Nature* **389**, 162–164 (1997).  
 [4] Saminadayar, L., Glattli, D. C., Jin, Y. & Etienne, B. Observation of the  $e/3$  Fractionally Charged Laughlin Quasiparticle. *Phys. Rev. Lett.* **79**, 2526–2529 (1997).

- [5] Nakamura, J., Liang, S., Gardner, G. C. & Manfra, M. J. Direct observation of anyonic braiding statistics. *Nat. Phys.* **16**, 931–936 (2020).
- [6] Bartolomei, H. *et al.* Fractional statistics in anyon collisions. *Science* **368**, 173–177 (2020).
- [7] Rosenow, B. & Halperin, B. I. Nonuniversal Behavior of Scattering between Fractional Quantum Hall Edges. *Phys. Rev. Lett.* **88**, 096404 (2002).
- [8] Papa, E. & MacDonald, A. H. Interactions Suppress Quasiparticle Tunneling at Hall Bar Constrictions. *Phys. Rev. Lett.* **93**, 126801 (2004).
- [9] Shtanko, O., Snizhko, K. & Cheianov, V. Nonequilibrium noise in transport across a tunneling contact between  $\nu = \frac{2}{3}$  fractional quantum Hall edges. *Phys. Rev. B* **89**, 125104 (2014).
- [10] Dolcetto, G., Barbarino, S., Ferraro, D., Magnoli, N. & Sasseti, M. Tunneling between helical edge states through extended contacts. *Phys. Rev. B* **85**, 195138 (2012).
- [11] Snizhko, K. & Cheianov, V. Scaling dimension of quantum Hall quasiparticles from tunneling-current noise measurements. *Phys. Rev. B* **91**, 195151 (2015).
- [12] Schiller, N., Oreg, Y. & Snizhko, K. Extracting the scaling dimension of quantum Hall quasiparticles from current correlations. *Phys. Rev. B* **105**, 165150 (2022).
- [13] Heiblum, M. *Fractional Charge Determination via Quantum Shot Noise Measurements*, 115–136 (in Perspectives of Mesoscopic Physics, Edited by A. Aharony and O. Antin-Wholman, World Scientific Publishing, 2010).
- [14] Nayak, C., Simon, S. H., Stern, A., Freedman, M. & Das Sarma, S. Non-Abelian anyons and topological quantum computation. *Rev. Mod. Phys.* **80**, 1083–1159 (2008).
- [15] Wen, X. G. *Quantum Field Theory of Many-Body Systems: From the Origin of Sound to an Origin of Light and Electrons* (Oxford University Press, Oxford, 2004).
- [16] Jain, J. *Composite Fermions* (Cambridge University Press, Cambridge, 2007).
- [17] Giamarchi, T. *Quantum Physics in One Dimension*. International Series of Monographs on Physics (Oxford University Press, 2004).
- [18] Jonckheere, T., Rech, J., Grémaud, B. & Martin, T. Anyonic Statistics Revealed by the Hong-Ou-Mandel Dip for Fractional Excitations. *Phys. Rev. Lett.* **130**, 186203 (2023).
- [19] Iyer, K. *et al.* The finite width of anyons changes their braiding signature (2023). ArXiv: 2311.15094.
- [20] Thamm, M. & Rosenow, B. Finite Soliton Width Matters: Investigating Non-equilibrium Exchange Phases of Anyons (2023). ArXiv: 2312.04475.
- [21] Reznikov, M., de Picciotto, R., Griffiths, T., Heiblum, M. & Umansky, V. Observation of quasiparticles with one-fifth of an electron’s charge. *Nature* **399**, 238–241 (1999).
- [22] Martin, J. *et al.* Localization of Fractionally Charged Quasi-Particles. *Science* **305**, 980–983 (2004).
- [23] Dolev, M., Heiblum, M., Umansky, V., Stern, A. & Mahalu, D. Observation of a quarter of an electron charge at the  $\nu = 5/2$  quantum Hall state. *Nature* **452**, 829–834 (2008).
- [24] Venkatachalam, V., Yacoby, A., Pfeiffer, L. & West, K. Local charge of the  $\nu = 5/2$  fractional quantum Hall state. *Nature* **469**, 185–188 (2011).
- [25] Kapfer, M. *et al.* A Josephson relation for fractionally charged anyons. *Science* **363**, 846–849 (2019).
- [26] Bisognin, R. *et al.* Microwave photons emitted by fractionally charged quasiparticles. *Nature Communications* **10**, 1708 (2019).
- [27] Rössli, M. P. *et al.* Fractional Coulomb blockade for quasi-particle tunneling between edge channels. *Science Advances* **7**, eabf5547 (2021).
- [28] Nakamura, J., Liang, S., Gardner, G. C. & Manfra, M. J. Fabry-Pérot Interferometry at the  $\nu = 2/5$  Fractional Quantum Hall State. *Phys. Rev. X* **13**, 041012 (2023).
- [29] Glidic, P. *et al.* Cross-Correlation Investigation of Anyon Statistics in the  $\nu = 1/3$  and  $2/5$  Fractional Quantum Hall States. *Phys. Rev. X* **13**, 011030 (2023).
- [30] Ruelle, M. *et al.* Comparing Fractional Quantum Hall Laughlin and Jain Topological Orders with the Anyon Collider. *Phys. Rev. X* **13**, 011031 (2023).
- [31] Lee, J.-Y. M. *et al.* Partitioning of diluted anyons reveals their braiding statistics. *Nature* **617**, 281 (2023).
- [32] Rosenow, B., Levkivskiy, I. P. & Halperin, B. I. Current Correlations from a Mesoscopic Anyon Collider. *Phys. Rev. Lett.* **116**, 156802 (2016).
- [33] Lee, J.-Y. M. & Sim, H.-S. Non-Abelian anyon collider. *Nature Communications* **13**, 6660 (2022).
- [34] Roddaro, S., Pellegrini, V., Beltram, F., Biasiol, G. & Sorba, L. Interedge Strong-to-Weak Scattering Evolution at a Constriction in the Fractional Quantum Hall Regime. *Phys. Rev. Lett.* **93**, 046801 (2004).
- [35] Radu, I. P. *et al.* Quasi-particle properties from Tunneling in the  $\nu = 5/2$  Fractional Quantum Hall State. *Science* **320**, 899 (2008).
- [36] Baer, S. *et al.* Experimental probe of topological orders and edge excitations in the second Landau level. *Phys. Rev. B* **90**, 075403 (2014).
- [37] Anthore, A. *et al.* Circuit Quantum Simulation of a Tomonaga-Luttinger Liquid with an Impurity. *Phys. Rev. X* **8**, 031075 (2018).
- [38] Cohen, L. A. *et al.* Universal chiral Luttinger liquid behavior in a graphene fractional quantum Hall point contact. *Science* **382**, 542–547 (2023).
- [39] Chang, A. M. Chiral Luttinger liquids at the fractional quantum Hall edge. *Rev. Mod. Phys.* **75**, 1449–1505 (2003).
- [40] Roddaro, S., Pellegrini, V., Beltram, F., Biasiol, G. & Sorba, L. Interedge Strong-to-Weak Scattering Evolution at a Constriction in the Fractional Quantum Hall Regime. *Phys. Rev. Lett.* **93**, 046801 (2004).
- [41] Lin, X., Dillard, C., Kastner, M. A., Pfeiffer, L. N. & West, K. W. Measurements of quasiparticle tunneling in the  $\nu = \frac{5}{2}$  fractional quantum Hall state. *Phys. Rev. B* **85**, 165321 (2012).
- [42] Yang, K. Field Theoretical Description of Quantum Hall Edge Reconstruction. *Phys. Rev. Lett.* **91**, 036802 (2003).
- [43] Ferraro, D., Braggio, A., Merlo, M., Magnoli, N. & Sasseti, M. Relevance of Multiple Quasiparticle Tunneling between Edge States at  $\nu = p/(2np+1)$ . *Phys. Rev. Lett.* **101**, 166805 (2008).
- [44] Rech, J., Jonckheere, T., Grémaud, B. & Martin, T. Negative Delta- $T$  Noise in the Fractional Quantum Hall Effect. *Phys. Rev. Lett.* **125**, 086801 (2020).
- [45] Zhang, G., Gornyi, I. V. & Spänslätt, C. Delta- $T$  noise for weak tunneling in one-dimensional systems: Interactions versus quantum statistics. *Phys. Rev. B* **105**, 195423 (2022).
- [46] Ebisu, H., Schiller, N. & Oreg, Y. Fluctuations in Heat

- Current and Scaling Dimension. *Phys. Rev. Lett.* **128**, 215901 (2022).
- [47] Kane, C. L. & Fisher, M. P. A. Impurity scattering and transport of fractional quantum Hall edge states. *Phys. Rev. B* **51**, 13449–13466 (1995).
- [48] Kamata, H., Kumada, N., Hashisaka, M., Muraki, K. & Fujisawa, T. Fractionalized wave packets from an artificial Tomonaga–Luttinger liquid. *Nature Nanotechnology* **9**, 177–181 (2014).
- [49] Batra, N. & Feldman, D. E. Different fractional charges from auto- and cross-correlation noise in quantum Hall states without upstream modes (2023). ArXiv: 2307.03713.
- [50] Blanter, Y. & Büttiker, M. Shot noise in mesoscopic conductors. *Phys. Rep.* **336**, 1–166 (2000).
- [51] Griffiths, T. G., Comforti, E., Heiblum, M., Stern, A. & Umansky, V. Evolution of Quasiparticle Charge in the Fractional Quantum Hall Regime. *Phys. Rev. Lett.* **85**, 3918–3921 (2000).
- [52] Muralidharan, B., Kumar, M. & Li, C. Emerging quantum hybrid systems for non-Abelian-state manipulation. *Front. Nanotechnol.* **5** (2023).
- [53] Davies, J. H. & Larkin, I. A. Theory of potential modulation in lateral surface superlattices. *Phys. Rev. B* **49**, 4800–4809 (1994).
- [54] Iftikhar, Z. *et al.* Primary thermometry triad at 6 mK in mesoscopic circuits. *Nat. Commun.* **7**, 12908 (2016).
- [55] Liang, Y., Dong, Q., Gennser, U., Cavanna, A. & Jin, Y. Input Noise Voltage Below  $1\text{ nV/Hz}^{1/2}$  at 1 kHz in the HEMTs at 4.2 K. *J. Low Temp. Phys.* **167**, 632–637 (2012).
- [56] Jezouin, S. *et al.* Quantum Limit of Heat Flow Across a Single Electronic Channel. *Science* **342**, 601–604 (2013).
- [57] Glidic, P. *et al.* Quasiparticle Andreev scattering in the  $\nu = 1/3$  fractional quantum Hall regime. *Nature Communications* **14**, 514 (2023).
- [58] Gross, Y., Dolev, M., Heiblum, M., Umansky, V. & Mahalu, D. Upstream Neutral Modes in the Fractional Quantum Hall Effect Regime: Heat Waves or Coherent Dipoles. *Phys. Rev. Lett.* **108**, 226801 (2012).
- [59] Bid, A., Ofek, N., Heiblum, M., Umansky, V. & Mahalu, D. Shot Noise and Charge at the  $2/3$  Composite Fractional Quantum Hall State. *Phys. Rev. Lett.* **103**, 236802 (2009).
- [60] Kane, C. L., Fisher, M. P. A. & Polchinski, J. Randomness at the edge: Theory of quantum Hall transport at filling  $\nu=2/3$ . *Phys. Rev. Lett.* **72**, 4129–4132 (1994).

**Data and code availability.** Plotted data, raw data and data analysis code are available on Zenodo: <https://doi.org/10.5281/zenodo.10599319>

**Acknowledgments.** This work was supported by the European Research Council (ERC-2020-SyG-951451) and the French RENATECH network. We thank K. Snizhko for discussions and E. Boulat for providing the  $\tau(V, T)$  prediction at  $\nu = 1/3$  in Fig. 2.

**Author Contributions.** A.V., C.P., P.G., Y.S. and F.P. performed the experiments with inputs from A.Aa. and A.An.; A.V. and F.P. analyzed the data with inputs from A.An., C.P., P.G. and Y.S.; A.C. and U.G. grew the 2DEG; A.V., A.Aa, and F.P. fabricated the sample; Y.J. fabricated the HEMT used in the cryogenic noise amplifiers; A.V. and F.P. wrote the manuscript with contributions from all au-

thors; A.An. and F.P. led the project.

**Author Information.** Correspondence and requests for materials should be addressed to A.An. (anne.anthore@c2n.upsaclay.fr) and F.P. (fred-eric.pierre@cnrs.fr).

*Note added.*— Coincident to the present investigation, two other works are experimentally addressing the scaling dimension of the  $e/3$  fractional quantum Hall quasiparticles at  $\nu = 1/3$ . An experiment by the team of M. Heiblum with a theoretical analysis led by K. Snizhko (N. Schiller *et al.*, in preparation) exploits the same thermal to shot noise crossover as in the present work, with a focus on low voltages and assuming the predicted fractional charge (see Fig. 5 for such a single parameter data analysis at low bias), and finds  $\Delta \simeq 1/2$ . The team of G. Feve (M. Ruelle *et al.*, submitted) relies on a different, dynamical response signature and finds  $\Delta \simeq 1/3$ . In these two coincident works the extracted scaling dimension is different from the pristine prediction  $\Delta = 1/6$ , which is observed in the present work. As pointed out in the manuscript, the emergence of non-universal behaviors could be related to differences in the geometry of the QPCs.

## METHODS

**Sample.** The sample is nanofabricated by e-beam lithography on a Ga(Al)As heterojunction forming a 2DEG buried at 140 nm, of density  $n = 1.2 \times 10^{11} \text{ cm}^{-2}$ , and of mobility  $1.8 \times 10^6 \text{ cm}^2 \text{ V}^{-1} \text{ s}^{-1}$ . The 2DEG mesa is first delimited by a wet etching of 105 nm, deeper than the Si  $\delta$ -doping located 65 nm below the Ga(Al)As surface. The large ohmic contacts are then formed by e-beam evaporation of a AuGeNi stack followed by a 50s thermal annealing at 440°C. A 15 nm layer of HfO<sub>2</sub> is grown by thermal ALD at 100°C over the entire mesa, in order to strongly reduce a gate-induced degradation of the 2DEG that could complicate the edge physics. This degradation is generally attributed to unequal thermal contractions upon cooling [53] or a deposition stress, which could also modulate the edge potential carrying the quantum Hall channels along the gates. The Ti (5 nm) - Au (20 nm) gates used to form the QPCs are evaporated on top of the HfO<sub>2</sub>. The split gates have a nominal tip-to-tip distance of 600 nm and a 25° tip opening angle prolonged until a gate width of 430 nm. The relatively important gate width (about three times the 2DEG depth) was chosen to reduce possible complications from Coulomb interactions between the quantum Hall edges across the gates [8, 48], and to better localize the tunneling location when the QPC is almost open (for less negative gate voltages) [10]. The nominal separation between the split gates controlling QPC<sub>w</sub> and the surrounding metal gate is 150 nm. Note that all the gates were grounded during the cooldown. Additional pictures of the sample are displayed in the Supplementary Information.

**Measurement setup.** The sample is cooled in a cryofree dilution refrigerator and electrically connected through measurement lines both highly-filtered and strongly anchored thermally (see [54] for details). Final RC filters with CMS components are positioned within the same metallic enclosure screwed to the mixing chamber that holds the sample: 200 k $\Omega$ -100 nF for gate lines, 10 k $\Omega$ -100 nF for the bias line, and 10 k $\Omega$ -1 nF for low frequency measurement lines. Note a relatively important filtering of the bias line, which prevents an artificial rounding of the thermal noise-shot noise crossover

from the flux noise induced by vibrations in a magnetic field. The differential QPC transmission  $\partial I_B/\partial I_{\text{inj}} = 1 - \partial I_F/\partial I_{\text{inj}}$  is measured by standard lock-in techniques at 13 Hz. A particularly small ac modulation is applied on  $V$  (of rms amplitude  $V_{\text{ac}}^{\text{rms}} \approx k_B T/3e$ ) to avoid any discernible rounding of the thermal noise-shot noise crossover. The transmitted and reflected dc currents are obtained by integrating with the applied bias voltage the corresponding lock-in signal  $I_{B,F}(V) = \int_0^V (\partial I_{B,F}/\partial V) dV$ .

Noise measurements are performed using specific cryogenics amplification chains connected to dedicated ohmic contacts, through nearly identical  $L - C$  tanks of resonant frequency 0.86 MHz [55, 56]. The noise ohmic contacts are located upstream of the ohmic contacts used for low frequency transmission measurements, as shown in Fig. 1. A dc block (2.2 nF) at the input of the  $L - C$  tanks preserves the low frequency lock-in signal. See Supplementary Information for a discussion of the relationship between measured noise and tunneling noise.

The device was immersed in a magnetic field close to the center of the corresponding Hall resistance plateaus, except when a shift  $\delta B$  is specifically indicated. The data at  $\nu = 1/3$ ,  $\nu = 2/5$ ,  $\nu = 2/3$  and  $\nu = 3$  were obtained at  $B = 13.7$  T (13.2 T for  $\delta B = -0.5$  T), 11.3 T, 6.8 T and 1.5 T, respectively. See Supplementary Information for the localization of these working points within a magnetic field sweep of the device.

**Thermometry.** The electronic temperature inside the device is ascertained by the noise measured at thermal equilibrium, with all QPCs closed. For temperatures  $T \geq 30$  mK (up to the maximum  $T \simeq 55$  mK), we find at  $\nu = 1/3$  and  $\nu = 3$  that the measured thermal noise is linear with the temperature readings of our calibrated RuO<sub>2</sub> thermometer. This establishes the good thermalization of electrons in the device with the mixing chamber, as well as the calibration of the RuO<sub>2</sub> thermometer. Accordingly, we indifferently get  $T \geq 30$  mK from the equilibrium noise or the equivalent RuO<sub>2</sub> readings. At the lowest probed temperatures  $\sim 15$  mK, the RuO<sub>2</sub> thermometers are no longer reliable and  $T$  is obtained from the thermal noise, by linearly extrapolating from  $S(T \geq 30$  mK). Note that the  $S(T)$  slope was not recalibrated at  $\nu = 2/3$ , but its change from  $\nu = 1/3$  was calculated from the separately obtained knowledge of the  $L - C$  tank circuit parameters, see ‘Noise amplification chains calibration’ below.

**Noise amplification chains calibration.** The gain factors  $G_{F,B}^{\text{eff}}$  between raw measurements of the auto-correlations, integrated within a frequency range  $[f_{\text{min}}, f_{\text{max}}]$ , and the power spectral density of current fluctuations  $\langle \delta I_{F,B}^2 \rangle$  are obtained from:

$$G_{F,B}^{\text{eff}} = \frac{s_{F,B}}{4k_B(1/R_{\text{tk}} + \nu e^2/h)}, \quad (3)$$

with  $R_{\text{tk}} \simeq 150$  k $\Omega$  the effective parallel resistance accounting for the dissipation in the considered  $L - C$  tank, and  $s_{F,B}$  the slope of the raw thermal noise versus temperature. The cross-correlation gain factor is simply given by  $G_{F,B}^{\text{eff}} \simeq \sqrt{G_F^{\text{eff}} G_B^{\text{eff}}}$ , up to a negligible reduction ( $< 0.5\%$ ) due to the small difference between the two  $L - C$  tanks. In practice, the thermal noise slopes  $s_{F,B}$  were only measured at  $\nu = 1/3$  and  $\nu = 3$ . The changes in  $G_{F,B}^{\text{eff}}(\nu)$  at  $\nu \in \{2/3, 2/5\}$  from the gains at

$\nu = 1/3$  are obtained from:

$$\frac{G_{F,B}^{\text{eff}}(\nu)}{G_{F,B}^{\text{eff}}(1/3)} = \frac{\int_{f_{\text{min}}}^{f_{\text{max}}} |Z_{\text{tk}}^{-1}(f) + \nu e^2/h|^{-2} df}{\int_{f_{\text{min}}}^{f_{\text{max}}} |Z_{\text{tk}}^{-1}(f) + e^2/3h|^{-2} df}, \quad (4)$$

with the tank impedance given by  $Z_{\text{tk}}^{-1}(f) = R_{\text{tk}}^{-1} + (iL_{\text{tk}}2\pi f)^{-1} + iC_{\text{tk}}2\pi f$ , where  $L_{\text{tk}} \simeq 250$   $\mu$ H and  $C_{\text{tk}} \simeq 135$  pF (see Methods in [57] for details regarding the calibration of the tank parameters). At  $\nu \in \{2/3, 2/5, 1/3\}$ , we integrated the noise signal in the same frequency window  $f_{\text{min}} = 840$  kHz and  $f_{\text{max}} = 880$  kHz. At  $\nu = 3$ , a larger window  $f_{\text{min}} = 800$  kHz and  $f_{\text{max}} = 920$  kHz takes advantage of the larger bandwidth  $\sim \nu e^2/2\pi h C_{\text{tk}}$ .

**Noise tests.** Among various experimental checks, we point out: (i) The effect of a dc bias voltage on the noise when each of the QPCs are either fully open or fully closed, which is here found below our experimental resolution. The presently imperceptible ‘source’ noise could have resulted from poor ohmic contact quality, incomplete electron thermalization in the contacts, dc current heating of the resistive parts of the bias line... (ii) The effect of the QPC transmission on the noise at zero dc bias voltage, which is here negligible at our experimental resolution. This rules out a possibly higher electron temperature in the ohmic contact connected to the bias line with respect to one connected to a cold ground, which would translate into an increase in  $\langle \delta I_B^2 \rangle$  at  $\tau = 1$  compared to  $\tau = 0$ . It also shows that the vibration noise in the bias line at frequencies well below 1 MHz does not translate into a discernible broadband excess shot noise for intermediate values of  $\tau$ .

**Fitting details.** The extracted values of  $e^*$  and  $\Delta$  shown in Fig. 3 (see Supplementary Information for the other gate voltage spans) represent the best fit parameters minimizing the variance between the shot noise data and Eq. 2. Only the meaningful points are displayed and included in the statistical analysis. These fulfill two conditions: (i) an accurate fit of the data can be achieved and (ii) the charge does not deviate too much from the expected value. Condition (i) requires a quantitative assessment of the fit accuracy. We used for this purpose the coefficient of determination  $R^2$  and chose to apply the same threshold to all the data taken in similar conditions. Specifically, we automatically discarded fits of  $R^2 < 0.9965$  at  $\nu = 1/3$  and for the outer channel at  $\nu = 2/5$ ,  $R^2 < 0.9966$  for the inner channel at  $\nu = 2/5$ , and  $R^2 < 0.9968$  at  $\nu = 2/3$ . The number of  $S(V)$  sweeps discarded by condition (i) is important, 2/3 of the total number (mostly when  $\tau$  is too close to 0 or 1). We checked that the overall results are only marginally affected by the specific threshold value (within reasonable variations). All the points that satisfy condition (i) are displayed and included in the statistical analysis of the quasiparticle charge. Condition (ii) is subsequently applied to deal with situations where the fitting charge is found at odds with the predicted value. Specifically we discarded  $S(V)$  sweeps for which the charge is found to be more than 44% off, i.e.  $e^* < 0.56e_{\text{th}}^*$  or  $e^* > 1.44e_{\text{th}}^*$ . The former happens at small  $\tau$  with a small QPC gate voltage. This gate voltage might not be enough to deplete the gas under the QPC gates, which could make tunneling happen in several places along the gates, and not only located at their tip, deviating from the model of a point contact. The latter occurs in the so-called strong back-scattering regime where the nature



of the tunneling quasiparticles is expected to change. Indeed, in the weak back-scattering regime ( $\tau \ll 1$ ) the tunneling barrier between the two edges is made of the electron gas in the fractional quantum Hall regime that selects the quasiparticles. However in the strong back-scattering regime ( $\tau \rightarrow 1$ ) the tunneling barrier between the two edges is made of vacuum that will select electrons. The points that do not satisfy condition (ii) are displayed with different symbols and not included in the statistical analysis of  $\Delta$ . They represent a small fraction (5%) of the data satisfying (i).

A complementary fitting procedure was employed to further establish the robustness of our results. In Fig. 5 we summarize the extracted  $\Delta$  obtained by fitting the thermal to shot noise crossover of  $S(V)$  using for  $e^*$  the theoretically predicted value. The fits are performed on the same set of  $S(V)$  sweeps as for the main fitting procedure for  $\Delta$  (obeying the two above mentioned conditions (i) and (ii)). The voltage bias extension of these fits is reduced to  $e^*|V| \leq 2k_B T$  to limit the weight of the shot noise solely sensitive to  $e^*$ .

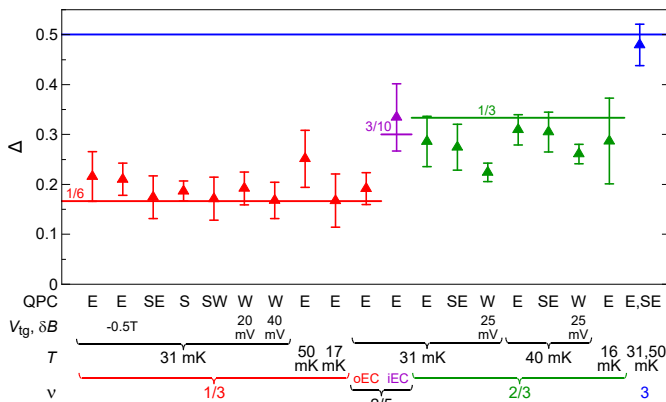


FIG. 5. **Summary of single parameter analysis.** Symbols recapitulate the extracted scaling dimension in all explored configurations, similarly to Fig. 4 but with  $\Delta$  obtained by a different procedure. The quasiparticle charge  $e^*$  is here assumed to take its predicted value, and the fit is performed solely on the thermal-shot noise crossover at low bias and using  $\Delta$  as only free parameter (see text).

**Filling factor 2/3.** In this more complex hole conjugate state [15, 16, 47] (i) the edges are not fully chiral and found to carry a backward heat current (going upstream the flow of electricity), and (ii) the QPCs often exhibit a plateau at half transmission (see e.g. [58, 59]). The former may introduce unwanted heat-induced contributions to the noise, while the latter allude to a composite edge structure with possible consequences on the interpretation of the noise signal.

(i) *Non-chiral heating.* As in previous works (see e.g. [58]), we observe in our device a non-chiral heating (only) at  $\nu = 2/3$ , through three noise signatures, see Fig. 6. (1) The strongest noise signal, seen at all temperatures, is obtained when the noise ohmic contact is electrically upstream a hot spot created  $\sim 30 \mu\text{m}$  downstream by applying a voltage to an adjacent ohmic contact (e.g. the contact normally used for measuring  $\langle I_B \rangle$  in Fig. 1, see Fig. 6a for a schematic of the configuration). See Fig. 3 of [58] for a similar observation

in the same configuration. Note that in configurations used for investigating  $\Delta$ , the noise measurement contacts are electrically upstream a floating contact (used to measure  $\langle I_{B,F} \rangle$ ) and, consequently, there is no such hot spot. (2) For the longer distance of  $\sim 150 \mu\text{m}$  between a hot spot in an ohmic contact and a QPC electrically upstream, a weaker noise signal from a different thermally induced partition mechanism can be detected at  $\tau \sim 0.5$  and only at the lowest temperature  $T \simeq 17 \text{ mK}$  (the same configuration is labeled N $\rightarrow$ C in Fig. 4 of [58], see Fig. 6b for a schematic of the configuration). The lower (imperceptible) effect at higher temperatures is expected assuming stronger heat exchanges between counter-propagating neutral and charge modes. Note that in the configurations used to probe  $\Delta$  the ohmic contacts electrically downstream the QPC are floating (used to measure the noise or  $\langle I_F \rangle$ ) and, consequently, there is no such hot spot. (3) A possibly more consequential signature of upstream heating is observed when using the configuration to probe  $\Delta$  through the increase in the noise sum  $S_\Sigma \equiv S_F + S_B + 2S_{FB}$ . From charge conservation and the chirality of electrical current,  $S_\Sigma$  corresponds to the thermal noise from the ohmic contacts electrically upstream the QPC (and not the direct partition noise at the QPC). In fully chiral states such as  $\nu \in \{1/3, 2/5, 3\}$  this temperature is independent of the applied bias  $V$ , and so is  $S_\Sigma$ . At  $\nu = 2/3$  and  $T \simeq 16 \text{ mK}$  this is not the case, which is interpreted as hot spots generated in the  $\sim 150 \mu\text{m}$  upstream ohmic contacts by neutral modes generated at the voltage-biased QPC (for a previous observation of the same mechanism, see configuration labeled C $\rightarrow$ N in Fig. 4 of [58], see Fig. 6c for a schematic of the configuration). In practice, we observe a fast increase followed by a near saturation at  $S_\Sigma \lesssim 710^{-30} \text{ A}^2 \text{ Hz}^{-1}$ , which is not negligible with respect to the partition noise of interest (see Fig. 2c). To limit the impact of this effect at  $T \simeq 16 \text{ mK}$  and  $\nu = 2/3$ , we only considered the cross-correlation signal ( $S \equiv -S_{FB} = -\langle \delta I_F \delta I_B \rangle$ ) measured on QPC<sub>E</sub>. Indeed, a symmetric heating of the two ohmic contacts electrically upstream of QPC<sub>E</sub> (biased at  $V$  and grounded) would not result in any change of the cross-correlations (but in a thermally induced increase of the auto-correlations). See [49] for a discussion regarding the increased robustness to artifacts of cross-correlations with respect to auto-correlations. At the higher probed temperatures, there was no discernible change in  $S_\Sigma$  and we performed our data analysis using all the noise measurements available.

(ii) *Noisy  $\tau = 1/2$  plateau.* A small plateau at  $\tau = 1/2$  is present in the transmission versus split gate voltage of both QPC<sub>E</sub> (see inset in Fig. 3c) and QPC<sub>SE</sub>. For specific voltages applied to the top gate (e.g.  $V_{tg} = -85 \text{ mV}$ ) a broad  $\tau = 1/2$  plateau can also develop on QPC<sub>W</sub> (other QPCs were not used at  $\nu = 2/3$ ). These plateaus, which are robust to the application of a bias voltage  $V$ , suggest the presence of two  $e^2/3h$  edge channels sequentially transmitted across the QPC. In that case there would be no partition noise at the QPC and one would naively expect an absence of shot noise. We do observe such noiseless plateaus at  $\nu = 3$  and  $\nu = 2/5$ . However, at  $\nu = 2/3$ , we find an important shot noise signal, effectively transparent to the presence of the plateau (see e.g. [59] for a previous observation of a noisy plateau at  $\nu = 2/3$ ). Accordingly, the QPC transmission is here defined as that of a single charge-carrying channel of conductance  $2e^2/3h$ , in agreement with the widespread theoretical description of the  $\nu = 2/3$  edge as one charge mode and one counter-propagating neutral mode [60].

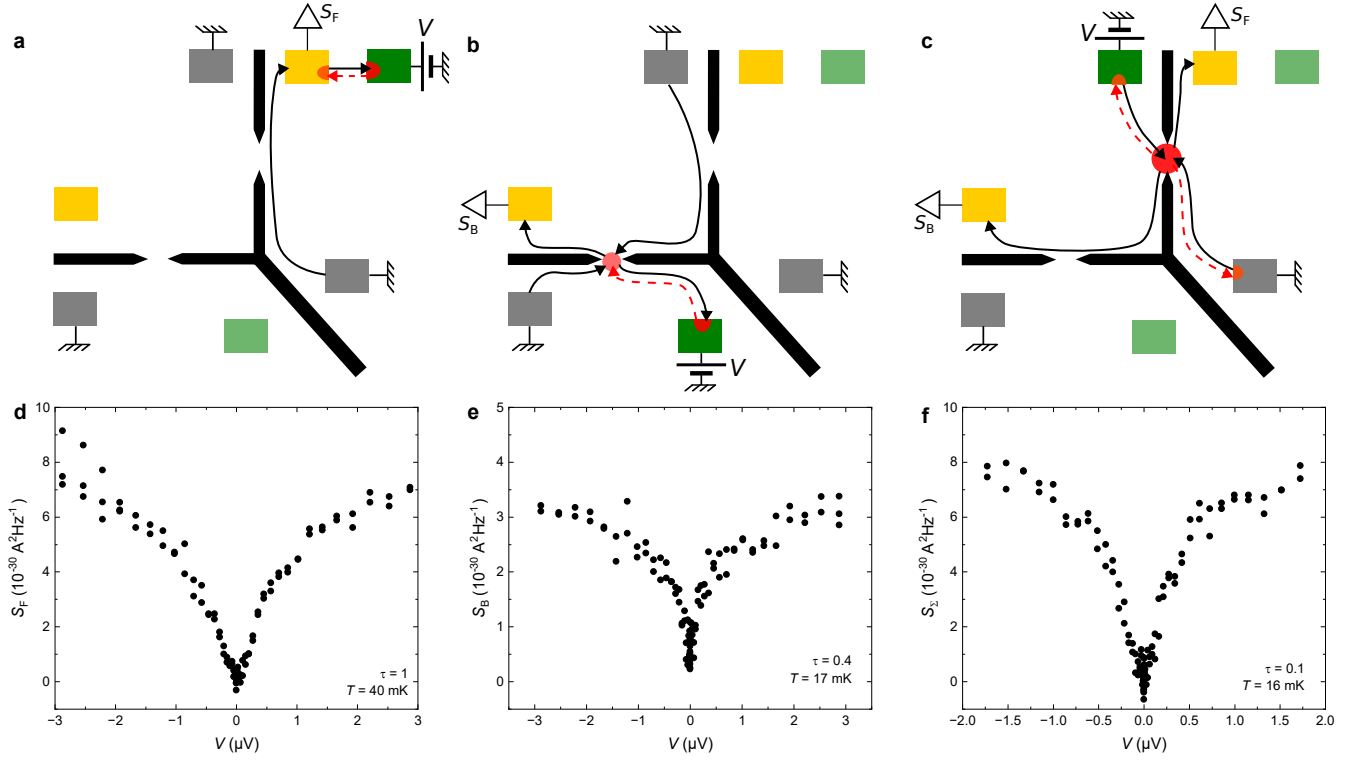


FIG. 6. **Signatures of upstream neutral heat flow at  $\nu = 2/3$ .** The presence of a neutral heat current flowing in the opposite direction of the electrical current is assessed by noise measurements in three different configurations. **a, b, c,** Schematic illustrations of the three processes (described in the text) by which heat is created, transported upstream by the neutral modes (red dashed arrows) and detected. **d, e, f,** Noise signature of upstream heating measured in the configuration displayed in the panel immediately above.

# Supplementary Information for 'Observation of the scaling dimension of fractional quantum Hall anyons'

A. Veillon,<sup>1</sup> C. Piquard,<sup>1</sup> P. Glidic,<sup>1</sup> Y. Sato,<sup>1</sup> A. Aassime,<sup>1</sup>  
A. Cavanna,<sup>1</sup> Y. Jin,<sup>1</sup> U. Gennser,<sup>1</sup> A. Anthore,<sup>1,2</sup> and F. Pierre<sup>1</sup>

<sup>1</sup> *Université Paris-Saclay, CNRS, Centre de Nanosciences et de Nanotechnologies, 91120, Palaiseau, France*

<sup>2</sup> *Université Paris Cité, CNRS, Centre de Nanosciences et de Nanotechnologies, F-91120, Palaiseau, France*

## I. SAMPLE

Larger-scale electron-beam and optical images of the measured device are displayed in Supplementary Figure **S1**. A high magnification picture of QPC<sub>W</sub> with its surrounding metal gate is shown in Supplementary Figure **S2**.

Supplementary Figure **S3** represents a magnetic field sweep along  $B \in [4, 14]$  T ( $\nu \in [1/3, 1]$ ) of the forward  $\tilde{V}_F$  and back-scattered  $\tilde{V}_B$  signals across a fully open QPC<sub>E</sub> (other QPCs are fully closed).

## II. SUPPLEMENTARY DATA

Individual values of  $\Delta$  and  $e^*/e$  extracted along gate voltage spans are displayed in Supplementary Figures **S4** and **S5**, in complement to Fig. 3 of the main text.

The dc voltage dependence of the transmission  $\tau(V)$  at all gate voltage tunings in the three configurations shown in Fig. 3 of the main text are plotted in Supplementary Figure **S6**. Among these are three  $\tau(V)$  also shown in the insets of Fig. 2a,b,c of the main text.

## III. RELATIONSHIP BETWEEN MEASURED NOISE AND TUNNELING NOISE

The measured back-scattered current  $I_B$  can always be written as the sum  $I_B = I_T + I_{\text{gnd}}$  of the incident current  $I_{\text{gnd}}$  emitted from the ohmic contact that would solely contribute to  $I_B$  in the absence of tunneling, and of the tunneling current  $I_T$  across the constriction. With this decomposition, the back-scattered current noise reads:

$$\langle \delta I_B^2 \rangle = \langle \delta I_T^2 \rangle + 2 \langle \delta I_T \delta I_{\text{gnd}} \rangle + \langle \delta I_{\text{gnd}}^2 \rangle, \quad (1)$$

with  $\langle \delta I_{\text{gnd}}^2 \rangle = 2k_B T \nu e^2 / h$  the thermal noise emitted from the grounded reservoir. Note that since  $\langle \delta I_{\text{gnd}}^2 \rangle$  is independent of the applied bias voltage  $V$ , it cancels in the excess noise  $S_B$ . In the tunneling limit ( $\tau_B \ll 1$ ), theory predicts from detailed balanced between upstream and downstream tunneling events that the first term in the right side of Eq. 1 is independent of the scaling dimension  $\Delta$  and given by [1]:

$$\langle \delta I_T^2 \rangle = 2e^* \langle I_B \rangle \coth \frac{e^* V}{2k_B T}. \quad (2)$$

The dependence on  $\Delta$  of the measured noise thus solely results from the second term on the right side of Eq. 1, namely  $2 \langle \delta I_T \delta I_{\text{gnd}} \rangle$ . According to the so-called non-equilibrium fluctuation-dissipation relations for chiral systems (assuming a  $V$ -independent Hamiltonian, as discussed below), this  $\Delta$  dependent contribution to the noise is simply given by [2]:

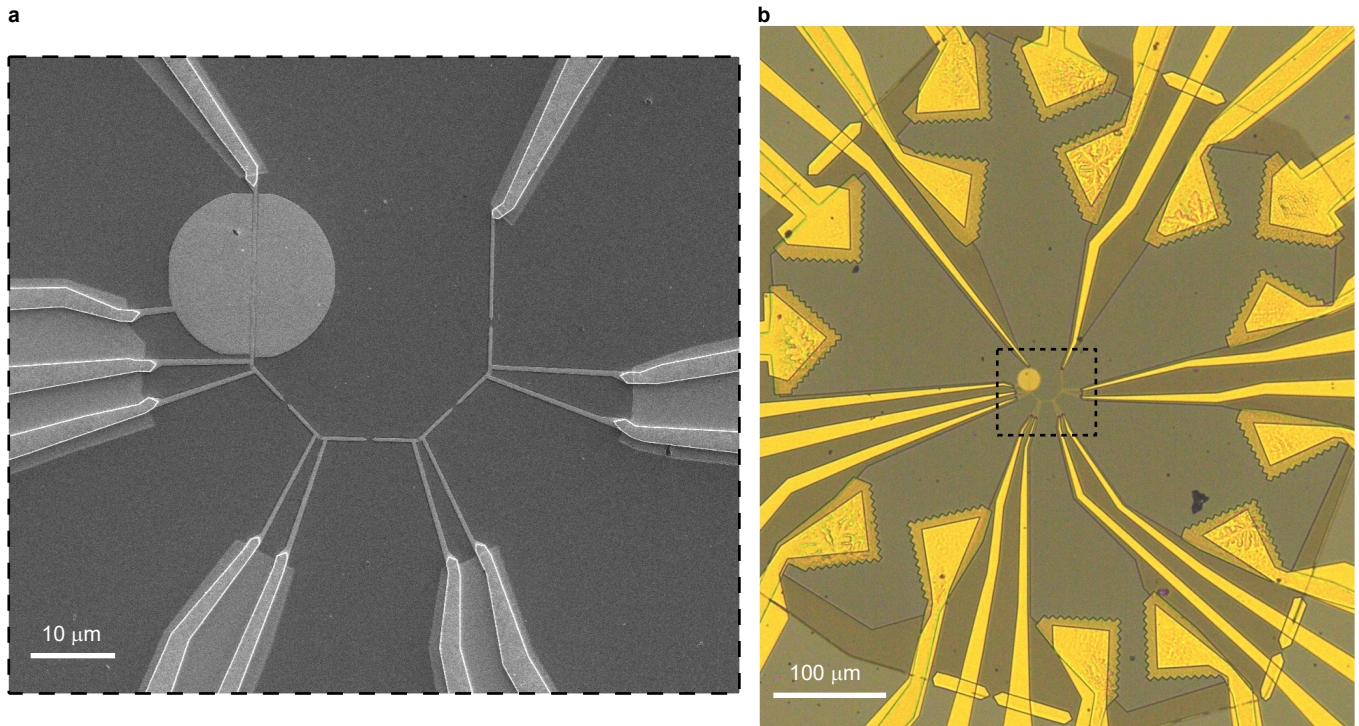
$$\langle \delta I_T \delta I_{\text{gnd}} \rangle = -2k_B T \frac{\partial \langle I_B \rangle}{\partial V}. \quad (3)$$

Experimentally,  $\partial \langle I_B \rangle / \partial V$  is directly measured. Hence, in this framework, one could calculate the excess noise  $S_B^{\text{FDT}}$  by plugging the separately measured tunneling current and its derivative into these equations. This gives (with in addition the usual ad hoc correction for large  $\tau$ )

$$S_B^{\text{FDT}} = 2e^*(1 - \tau) \langle I_B \rangle \coth \frac{e^* V}{2k_B T} - 4k_B T \left( 1 - \frac{\partial \langle I_B \rangle}{\partial I_{\text{inj}}} \right) \frac{\partial \langle I_B \rangle}{\partial V}. \quad (4)$$

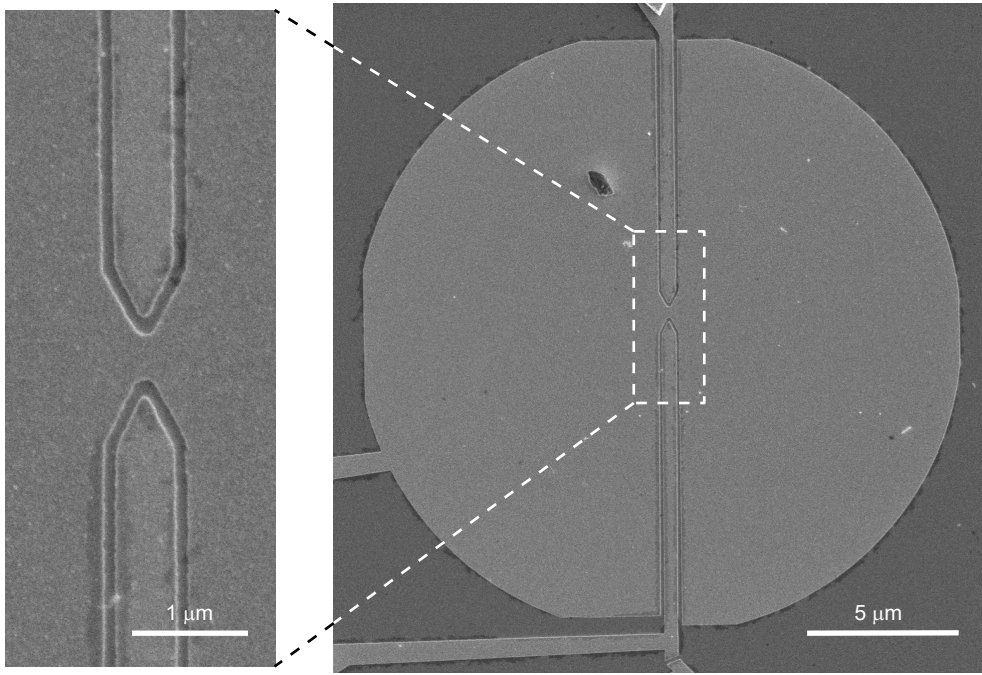
However, as illustrated in Supplementary Fig. **S7**, we find that Eq. 4 using the measured  $\langle I_B \rangle(V)$  does not reproduce the simultaneously measured thermal to shot noise crossover. This should not come as a surprise since the current,

and its derivative, do not follow Luttinger liquid predictions. One could explain this mismatch by invoking the same possible explanation as for the data-theory discrepancy on the  $I - V$  characteristics, namely that the shape of the QPC potential, and therefore the quasiparticle tunneling amplitude, is impacted by external parameters, such as an electrostatic deformation induced by a change in the applied bias voltage, the temperature or the tunneling current itself [3]. Indeed, as pointed-out in [2], Eq. 3 holds if the voltage bias  $V$  only manifests through the chemical potential of the incident edge channel, and not if applying  $V$  impacts the tunnel Hamiltonian.

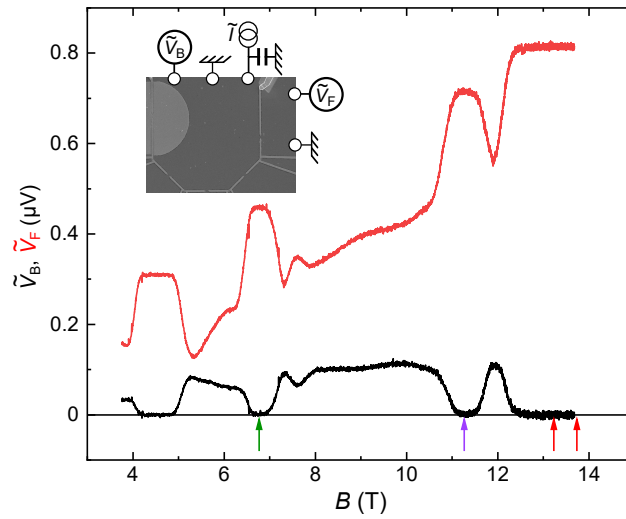


**Supplementary Figure S1. Large scale pictures of measured device.** **a**, electron-beam micrograph. Areas with a 2DEG underneath (the mesa) appear darker. Lighter parts with bright edges are thick gold layers used to climb down the mesa edges and as bonding pads. **b**, optical image. The thick top layer made of gold appears as the brightest yellow. Ohmic contacts have staircase edges and show as a darker shade of yellow. The surface over which the  $\text{HfO}_2$  was deposited (dark grey) completely encapsulates the active part of the device, including ohmic contacts. The dashed rectangle indicates the boundary of the electron-beam image in panel a.

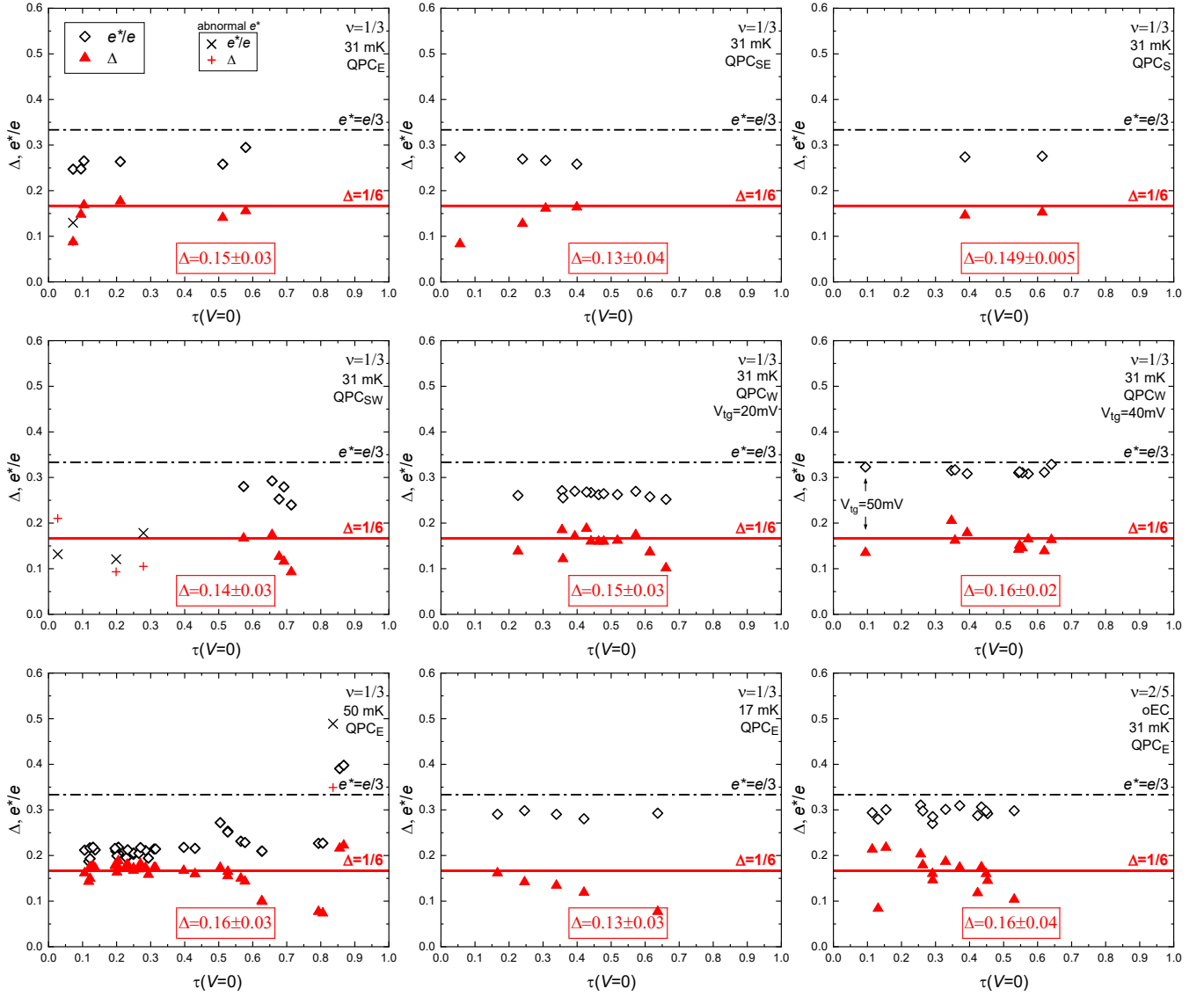
- 
- [1] Levitov, L. S. & Reznikov, M. Counting statistics of tunneling current. *Phys. Rev. B* **70**, 115305 (2004).  
 [2] Wang, C. & Feldman, D. E. Fluctuation-dissipation theorem for chiral systems in nonequilibrium steady states. *Phys. Rev. B* **84**, 235315 (2011).  
 [3] Shtanko, O., Snizhko, K. & Cheianov, V. Nonequilibrium noise in transport across a tunneling contact between  $\nu = \frac{2}{3}$  fractional quantum Hall edges. *Phys. Rev. B* **89**, 125104 (2014).



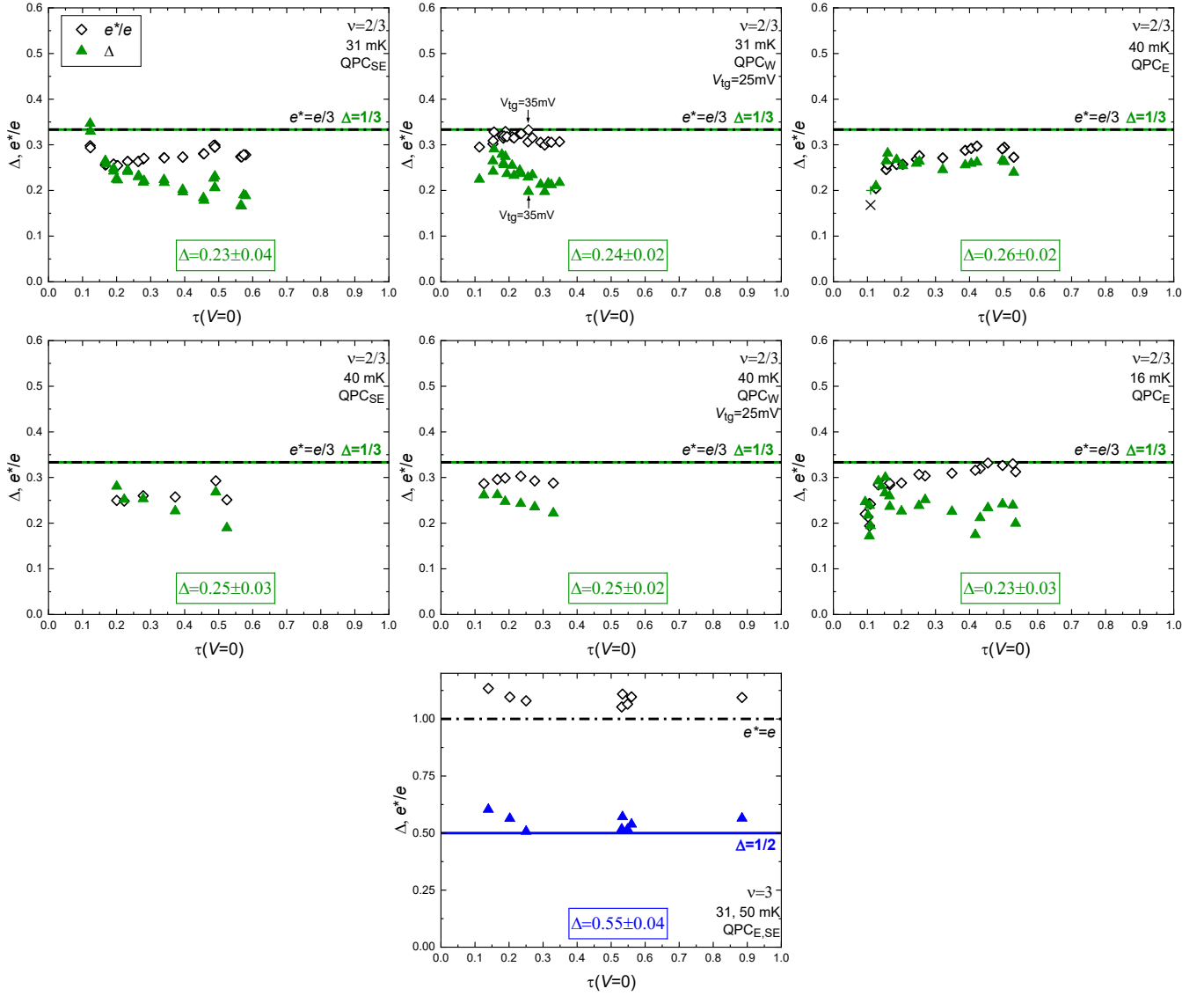
**Supplementary Figure S2. Quantum point contact with surrounding metal gate.** Electron-beam micrographs of QPC<sub>W</sub>.



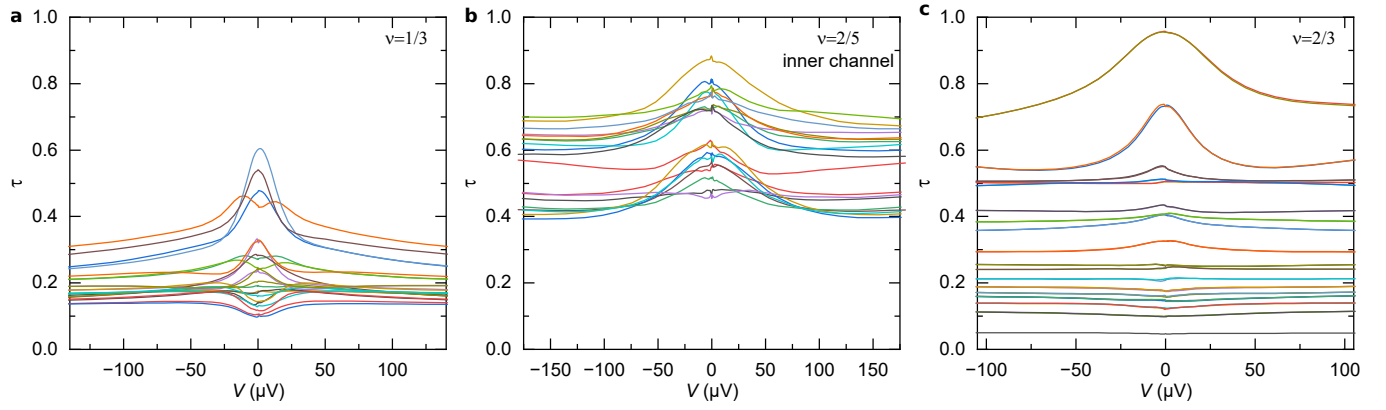
**Supplementary Figure S3. Magnetic field sweep.** Forward ( $\tilde{V}_F$ , red) and back-scattered ( $\tilde{V}_B$ , black) ac voltages across a fully open QPC<sub>E</sub>, in response to a fixed ac bias current  $\tilde{I}$ , are plotted as a function of magnetic field  $B$ . The other QPCs are fully closed. Arrows indicate at which  $B$  the different measurements were performed (except  $B \simeq 1.5$  T at  $\nu = 3$ , not shown here). At these points the back-scattered signal is zero whereas the forward signal is well within a plateau, despite the increased mixing chamber temperature of 160 mK during this  $B$  sweep. Note that  $\tilde{V}_F$  does not precisely scale as  $h/\nu e^2$  along plateaus, due to the parallel capacitance shown schematically (100 nF) and the finite ac frequency (13 Hz).



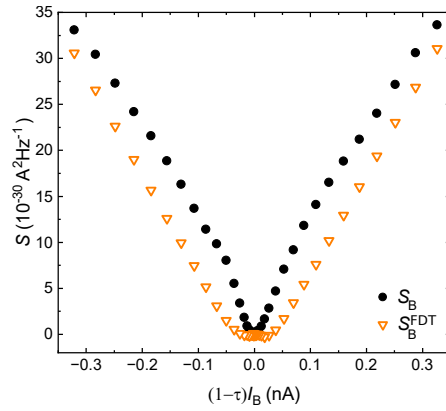
**Supplementary Figure S4. Scaling dimension vs QPC tuning of predicted  $\{e/3, \Delta = 1/6\}$  quasiparticles.** Individual values of extracted scaling dimension ( $\blacktriangle$ ) and charge ( $\diamond$ ) are plotted vs  $\tau(V=0)$  for each configuration addressing the predicted  $\{e/3, \Delta = 1/6\}$  fractional quantum Hall quasiparticles. A few points associated with anomalously low or high charge are shown as different symbols ( $+$ ,  $\times$ ). Each panel corresponds to the configuration indicated within it. The average and spread of  $\Delta$  indicated in the panels are calculated only on points displayed as  $\blacktriangle$  and correspond to the individual symbols with error bars in Fig. 4 of the main article. All measurements are here at  $\nu = 1/3$  except the bottom right panel addressing the outer edge channel at  $\nu = 2/5$ . The configuration corresponding to  $\{\nu = 1/3, \text{QPC}_E, 31 \text{ mK}, \delta B \simeq -0.5 \text{ T}\}$  is displayed in Fig. 3a of the main article.



**Supplementary Figure S5. Scaling dimension vs QPC tuning at  $\nu = 2/3$  and  $\nu = 3$ .** Individual values of extracted scaling dimension  $\Delta$  ( $\blacktriangle$ ) and charge  $e^*/e$  ( $\diamond$ ) are plotted vs  $\tau(V=0)$ . A few points associated with anomalously low or high charge are shown as different symbols ( $+$ ,  $\times$ ). Each panel corresponds to the configuration indicated within it. The average and spread of  $\Delta$  indicated in the panels are calculated only on points displayed as  $\blacktriangle$  and correspond to the individual symbols with error bars in Fig. 4 of the main article. The six top panels correspond to  $\nu = 2/3$  whereas the bottom one corresponds to  $\nu = 3$ . The configuration corresponding to  $\{\nu = 2/3, \text{QPC}_E, 31 \text{ mK}\}$  is displayed in Fig. 3c of the main article.



**Supplementary Figure S6. Transmission vs dc voltage bias at different gate voltages.** The measured QPC ‘backscattering’ transmission  $\tau$  is plotted vs  $V$  for the different gate voltage tunings and three QPC<sub>E</sub> configurations displayed in Fig. 3 of the main text. Each individual tuning in each panel is shown as a line of a different color. Panels **a,b,c** correspond to the  $\nu = 1/3$ ,  $2/5$  inner channel and  $2/3$  configurations displayed in Fig. 3a,b,c of the main article, respectively.



**Supplementary Figure S7. Measured  $S_B$  vs calculated  $S_B^{\text{FDT}}$ .** Illustrative comparison at  $\nu = 1/3$  between the measured excess noise  $S_B$  and the value  $S_B^{\text{FDT}}$  calculated from Eq. 4 (derived with the non-equilibrium fluctuation-dissipation relation Eq. 3) using the simultaneously measured  $\langle I_B \rangle(V)$ . The noise displayed here is the same as Fig. 2a of the main article. The mismatch could be explained by the same mechanism invoked for the  $I - V$  characteristics (see text).